AGU100 ADVANCING EARTH AND SPACE SCIENCE

Geophysical Research Letters

RESEARCH LETTER
10.1029/2018GL080763

**Key Points:**
- Ocean observations that are unprecedented in their spatial detail and proximity to a Greenlandic tidewater glacier are reported
- Despite being highly localized, plumes drive fjord-wide circulation and hence glacier-wide submarine melting at tidewater glaciers
- Fjord-scale submarine melting drives significant mass loss and may promote calving, hence is a key process determining glacier stability

**Supporting Information:**
- Supporting Information S1
- Data Set S1

**Correspondence to:**
D. A. Slater,
daslater@ucsd.edu

**Citation:**
Slater, D. A., Straneo, F., Das, S. B., Richards, C. G., Wagner, T. J. W., & Nienow, P. W. (2018). Localized plumes drive front-wide ocean melting of a Greenlandic tidewater glacier. *Geophysical Research Letters*, *45*, 12,350–12,358. https://doi.org/10.1029/2018GL080763

Received 4 OCT 2018
Accepted 11 NOV 2018
Accepted article online 15 NOV 2018
Published online 27 NOV 2018



# Localized Plumes Drive Front-Wide Ocean Melting of A Greenlandic Tidewater Glacier

**D. A. Slater[1], F. Straneo[1], S. B. Das[2], C. G. Richards[3], T. J. W. Wagner[4], and P. W. Nienow[5]**

[1]Scripps Institution of Oceanography, USA, [2]Woods Hole Oceanographic Institution, USA, [3]Bedford Institute of Oceanography, Canada, [4]Department of Physics and Physical Oceanography, University of North Carolina Wilmington, USA, [5]School of Geosciences, University of Edinburgh, UK

**Abstract** Recent acceleration of Greenland's ocean-terminating glaciers has substantially amplified the ice sheet's contribution to global sea level. Increased oceanic melting of these tidewater glaciers is widely cited as the likely trigger, and is thought to be highest within vigorous plumes driven by freshwater drainage from beneath glaciers. Yet melting of the larger part of calving fronts outside of plumes remains largely unstudied. Here we combine ocean observations collected within 100 m of a tidewater glacier with a numerical model to show that unlike previously assumed, plumes drive an energetic fjord-wide circulation which enhances melting along the entire calving front. Compared to estimates of melting within plumes alone, this fjord-wide circulation effectively doubles the glacier-wide melt rate, and through shaping the calving front has a potential dynamic impact on calving. Our results suggest that melting driven by fjord-scale circulation should be considered in process-based projections of Greenland's sea level contribution.

**Plain Language Summary** As the world warms, loss of ice from the Greenland Ice Sheet will be a significant source of sea level rise. Greenland loses ice partly through the flow of huge rivers of ice called tidewater glaciers that dump solid ice directly into the ocean. Over the past two decades, tidewater glaciers around Greenland have accelerated dramatically, increasing Greenland's contribution to global mean sea level. There is mounting evidence that these accelerations have been driven by ocean warming, and a resulting increase in the rate at which the ocean melts the front of tidewater glaciers (called submarine melting). Yet submarine melting is at present poorly understood, in part due to the danger and difficulty of collecting data close to tidewater glaciers. We present observations of the ocean in front of a tidewater glacier that are unprecedented in their proximity to the glacier. These data reveal an ocean circulation which flushes warm water along the front of the glacier, driving high rates of submarine melting. We then use a numerical model to identify what drives this circulation. Our results are an important step toward understanding a key process which will modulate future sea level contribution from the Greenland ice sheet.

## 1. Introduction

Loss of ice mass from the Greenland Ice Sheet is a major contributor to sea level rise. The ice sheet contributed ~12 mm to sea level from 1991 to 2015 (van den Broeke et al., 2016) and accounted for a fifth of global mean sea level rise between 2005 and 2014; a fraction which is expected to grow throughout the 21st century (Chambers et al., 2017). Approximately 40% of recent ice loss from Greenland stems from the flow of ice into the ocean at tidewater glaciers (van den Broeke et al., 2016). Accompanied by substantial atmospheric and oceanic warming (Box et al., 2009; Straneo & Heimbach, 2013), this flow has accelerated dramatically in recent decades (Moon et al., 2012). Given the expectation of continued climate warming over the coming decades, there is clear potential for significant further sea level contribution from Greenland's tidewater glaciers (Nick et al., 2013; Yin et al., 2011). Understanding the processes linking climate to tidewater glacier dynamics is thus fundamental to accurate sea level rise predictions.

The observed changes at tidewater glaciers have been widely attributed to an increase in submarine melting—that is, the rate at which the ocean melts the front of the glacier (Holland et al., 2008; Luckman et al., 2015; Straneo & Heimbach, 2013). If sufficiently rapid, submarine melting may directly drive glacier retreat, resulting in a dynamic response comprising acceleration, thinning, and longer-term further retreat

(Morlighem et al., 2016). Alternatively, submarine melting may change the shape of the calving front, thus altering the stress regime of the glacier and promoting calving (Chauché et al., 2014; Fried et al., 2015, 2018; O'Leary & Christoffersen, 2013; Rignot et al., 2015; Wagner et al., 2016; Xie et al., 2016). Such processes may provide a mechanism for submarine melting to be the driver of glacier retreat even when mass loss due to submarine melting is much smaller than that due to iceberg calving, as is likely the case at Greenland's largest tidewater glaciers (Moon et al., 2018). Despite its importance to glacier dynamics and sea level change, we still lack sufficient understanding of submarine melting.

Theoretically, submarine melt rates are primarily determined by two factors: glacier-adjacent water temperature and water motion (Holland & Jenkins, 1999), with the latter facilitating the turbulent transfer of available ocean heat to the ice. At the ice edge, both modeling and observational studies (Mankoff et al., 2016; Xu et al., 2012) suggest that during the summer, the dominant driver of water motion close to Greenlandic tidewater glaciers is the injection into the fjord of runoff derived from melting of the ice sheet surface. This buoyant runoff emerges from beneath the glacier, often hundreds of meters underwater, and results in a vigorous rising plume and high glacier-adjacent water velocities (Jenkins, 2011). As it rises the plume furthermore entrains surrounding fjord water and contributes to a two-dimensional estuarine-type circulation in the fjord whereby water is drawn toward the glacier at depth and flows away from the glacier closer to the surface (Carroll et al., 2015; Motyka et al., 2003).

Plumes have become the subject of intensive study, both due to their potential to drive rapid submarine melting of several meters per day (Slater et al., 2015) and their role in replenishing oceanic heat in the fjord (Cowton et al., 2015; Straneo et al., 2011). Yet given a characteristic plume width of ~100 m (Jackson et al., 2017; Mankoff et al., 2016; Slater et al., 2016) compared to typical calving fronts wider than 3 km, an individual plume occupies only a small fraction of the glacier calving front (<5%). This means that the majority of the calving front is not directly exposed to melting within a plume, and instead melting must occur either by unforced (melt-driven) convection, which is thought to be very weak (Magorrian & Wells, 2016), or due to any additional fjord-wide circulation (Bartholomaus et al., 2013). The presence of such a fjord-wide circulation, however, has not been quantitatively observed largely due to the challenge of obtaining measurements, especially of water velocity, close to tidewater glaciers.

This scarcity of ocean observations proximal to tidewater glaciers, combined with a lack of realistic models, has precluded quantification of the melting driven by fjord-wide circulation at Greenlandic tidewater glaciers. Much of our understanding of tidewater glacier submarine melting therefore derives from models of plume dynamics (Carroll et al., 2016; Slater et al., 2017), and current parameterizations of submarine melting at tidewater glaciers (Rignot et al., 2016; Todd et al., 2018) used in process studies thus neglect fjord-wide circulation. Given the large ice-ocean contact area affected, such melting may be significant in terms of total mass loss and in the potential to drive calving. In this study we pair ocean observations with numerical modeling to isolate fjord-wide circulation at a fjord-glacier system in west Greenland. While the glacier is slower-flowing than Greenland's largest glaciers (e.g., Helheim), the smaller calving flux means that the near-ice region is not rendered impassable by a thick ice mélange, allowing us to obtain ocean measurements which are unprecedented in their spatial detail and proximity to the calving front. We map the fjord-wide circulation, identify its drivers, and quantify its impact on submarine melting.

## 2. Field Site and Methods

Saqqarliup Sermia and Sarqardleq Fjord form a tidewater glacier-fjord system in west Greenland (Figure 1a). The 5-km-wide glacier flows into the fjord with ice velocity reaching 600 m/year at the calving front, while mapping of fjord bathymetry undertaken by Stevens et al. (2016) show the glacier is grounded in ~150 m of water (Figure 1b). The fjord connects the glacier to Ilulissat Icefjord, Disko Bay, and ultimately Baffin Bay. Two field campaigns in Sarqardleq Fjord, conducted in summer 2012 and 2013, show that waters adjacent to the glacier consist of ~1 °C Arctic-origin water overlain by a thin seasonally warm (7 °C) surface layer (Mankoff et al., 2016; Stevens et al., 2016). These surveys also revealed the existence of two plumes (Figure 1b); a primary plume in the center-west of the calving front driven by a summer runoff of ~100 $m^3/s$ and a secondary, weaker plume on the east side of the calving front resulting from a runoff of ~15 $m^3/s$ (Mankoff et al., 2016; Stevens et al., 2016).

The data presented in this paper (Figure 1b) were collected between 25 and 27 July 2013, during which period the primary plume was visible at the fjord surface due to its high sediment content. Water velocity was mea-

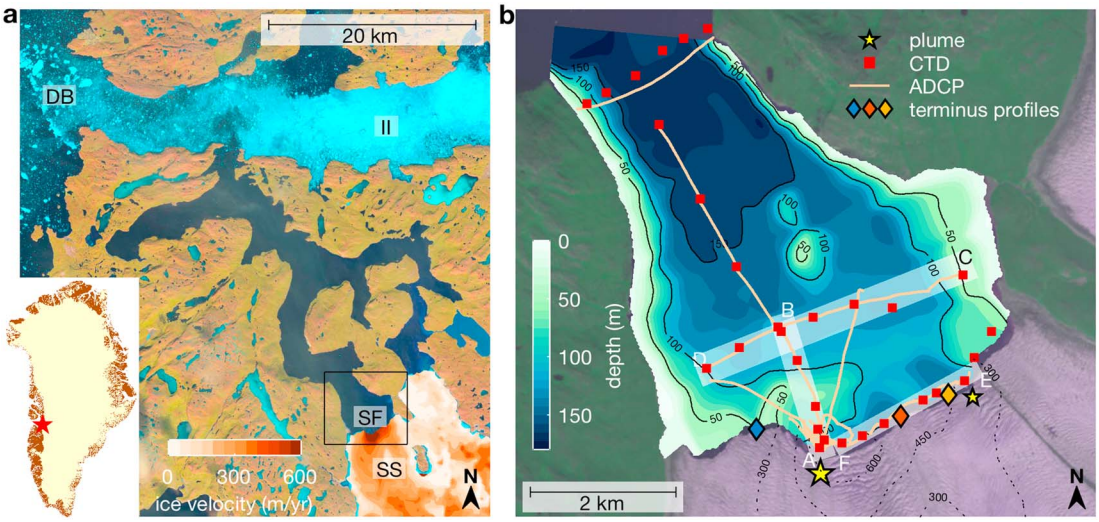


**Figure 1. Overview of the SF-SS system.** (a), Location in West Greenland. SS flows into SF, which is connected to DB via II. The background is a Landsat 8 image from 21 June 2013. Also shown is the mean 5 to 21 June 2013 ice velocity (Fahnestock et al., 2015; Scambos et al., 2016). The location of panel (b) is shown in the black box. (b) Bathymetry of the inner fjord (Stevens et al., 2016). Shown are the locations of the two plumes and the locations of water temperature and salinity measurements (conductivity-temperature-depth), current velocity observations (Acoustic Doppler Current Profiler), and calving front shape data (terminus profiles). Three transects—AB, CD, and EF—are referred to throughout the paper. Dashed contours over the glacier denote ice velocity in meters per year. The background is an ASTER image from 15 July 2013. SS = Saqqarliup Sermia; SF = Sarqardleq Fjord; DB = Disko Bay; II = Illulissat Icefjord.

sured using an Acoustic Doppler Current Profiler along several transects throughout the inner fjord, within 100 m of the glacier front and inside the surface expression of the primary plume. Similar transects of water temperature and salinity were observed with a number of conductivity-temperature-depth casts. The calving front shape profiles result from a multibeam sonar survey of the calving front made from a remote-controlled surface vehicle (Kimball et al., 2014).

To examine the drivers of the observed circulation and to quantify its effect on submarine melting of the glacier, we ran a high-resolution simulation of the fjord in the Massachusetts Institute of Technology general circulation model (MITgcm) (Marshall et al., 1997). The model includes the realistic bathymetry and fjord stratification (Figure 1b). Horizontal resolution is 20 m for the 2 km closest to the glacier, while vertical resolution is 1.5 m in the top 30 m, thereafter telescoping to 5 m at depth. We use Smagorinsky and KPP schemes to set eddy viscosities (Large et al., 1994; Smagorinsky, 1963). The model is forced only by the two plumes (Figure 1b), which are represented by boundary conditions on velocity, temperature, and salinity. For the primary plume, these are set using measurements of the plume (Mankoff et al., 2016) and thus include a flux of 1,750 $m^3/s$ of anomalously dense and cold water into the domain (away from the glacier) near the surface and a flux of 1,650 $m^3/s$ out of the domain (into the glacier) at depth. Detailed observations of the secondary plume are not available and we thus set boundary conditions based on buoyant plume theory (Slater et al., 2016), imposing a flux of 650 $m^3/s$ into the domain at the plume neutral buoyancy depth of ~35 m, and a flux of 635 $m^3/s$ out of the domain below. The model is run for 10 days and all results shown are outputs averaged over the tenth day. Further details on the data and model may be found in supporting information.

## 3. Results

### 3.1. Fjord Circulation

Water velocity observations along transect AB show water from the primary plume flowing away from the glacier in the top 30 m of the fjord as a jet with high velocity, reaching 2 m/s close to the glacier (Figure 2a). At the mid-fjord transect CD the jet is visible as a ~1 km wide region in the center of the fjord trending to the east and carrying a volume flux ~6,000 $m^3/s$. The jet is once more visible at the east side of the fjord in the velocity measurements furthest from the glacier, where the velocity has dropped to ~0.2 m/s. To each side of the jet, and particularly along transect EF, flow converges toward the jet generating an east to west flow along the central portion of the calving front (Figure 2a).

From 30 to 70 m depth, the circulation is almost exclusively directed toward the glacier at all measured points in the fjord (Figure 2b). The exceptions are a small region in the far east of the fjord on transect CD, which

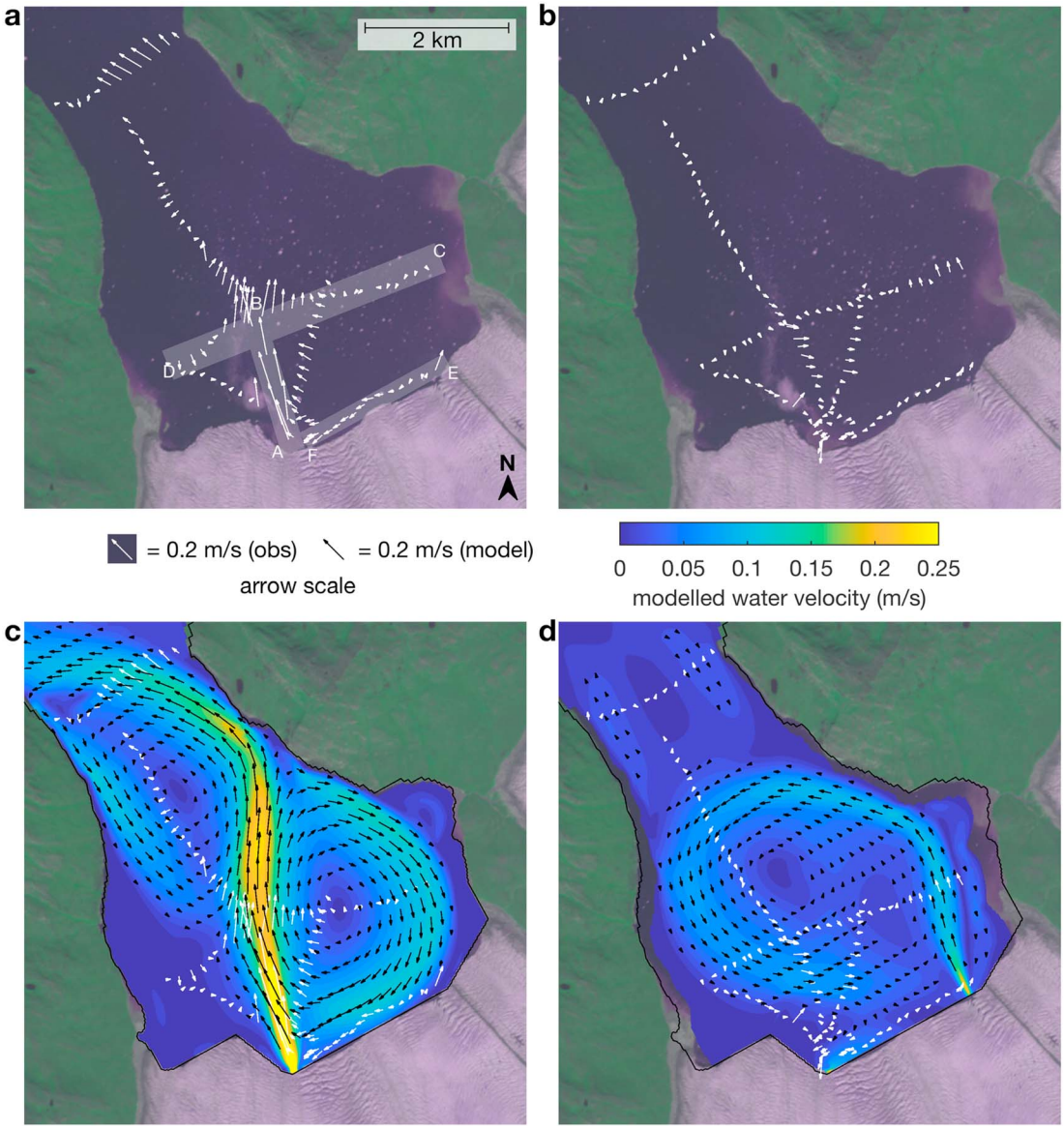


**Figure 2. Observed (a–b) and modeled (c–d) circulation at a fjord scale.** (a) Observed water velocity depth-averaged from the surface to 30 m depth, and (b) the equivalent plot for 30 to 70 m depth. The three transects from Figure 1b are repeated on (a) for ease of reference; transect EF coincides with the sections shown in Figure 3. (c) Modeled fjord circulation in the surface to 30 m depth range, as shown by the shading and the black arrows. Only modeled velocities exceeding 0.02 m/s are assigned arrows. A selection of the velocity observations are overlain as white arrows. (d) The equivalent plot for 30 to 70 m depth.

shows motion away from the glacier, and the calving front section EF, which shows velocities tangential to the calving front directed to both the east and the west (Figure 2b).

Water velocities modeled in MITgcm (Figure 2c) clearly show a jet confined to the upper 30 m of the fjord, which curves eastward as it proceeds away from the glacier and eventually bifurcates at the fjord wall, with the stronger flow continuing toward the ocean and the remainder recirculating back toward the glacier on the east side of the fjord. This recirculating flow runs westward parallel to the glacier before being re-entrained into the jet. From 30 to 70 m depth, the model shows a largely geostrophic counterclockwise circulation in the widest part of the fjord (Figure 2d; Supporting information), with flow away from the glacier confined to a narrow jet in the east of the fjord, and flow otherwise directed toward the glacier.

Given that the model is forced only by the two plumes, the fact that it captures the major features of the observed circulation (Figures 2c–2d), including the spatial variability and magnitude of observed current velocities, indicates that the fjord-scale circulation observed during the survey arises due to the presence of

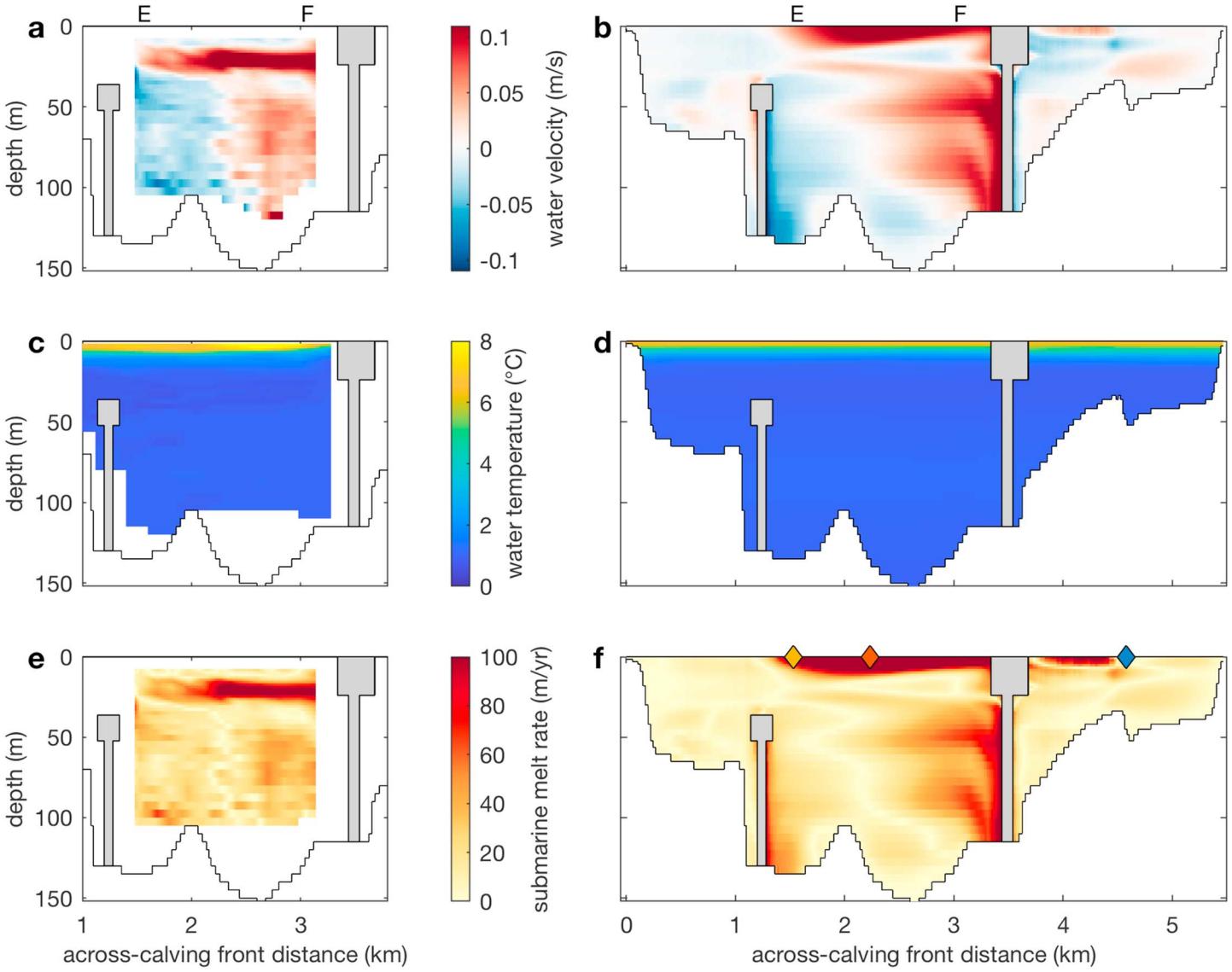


**Figure 3. Outside-of-plume submarine melting driven by fjord-wide circulation.** (a) Observed ice-tangential water velocity adjacent to the glacier along the transect EF shown in Figure 1b. The section is orientated so that the reader is looking toward the glacier. Positive velocities indicate flow from left to right (i.e., from east to west along the calving front). The gray vertical columns indicate the two plumes, while the solid black line indicates the bathymetry/grounding line. (b) Modeled ice-tangential water velocity adjacent to the ice over the full calving front. (c) Observed water temperature along the transect EF. (d) Modeled water temperature adjacent to the ice over the full calving front.
(e) Submarine melt rate along the transect EF, as estimated from the observed water velocity and temperature (Holland & Jenkins, 1999). (f) Modeled outside-of-plume submarine melt rate. The diamonds in (f) indicate the location (see also Figure 1b) of the calving front shape profiles shown in Figure 4a.

the two plumes. Specifically, the outflowing jet and recirculation eddy in the upper 30 m of the fjord are driven by the primary plume while the deeper outflow and resulting circulation are driven by the secondary plume (Figure 2).

The good agreement between the model and observations also holds adjacent to the ice along the transect EF where water velocity is elevated by the recirculations associated with the plumes (Figures 2 and 3a–3b). Over the upper 30 m, the recirculation eddy associated with the primary plume (Figure 2c) drives strong along-ice flow directed toward the primary plume (Figures 3a–3b), reaching 0.14 m/s in the model and 0.19 m/s in the observations. This recirculating flow is found ~15 m deeper in the observations relative to the model; we attribute this small difference to the fact that the model does not fully resolve the dynamics of the plume (supporting information). Nevertheless, the thickness, magnitude, and direction of the modeled and observed

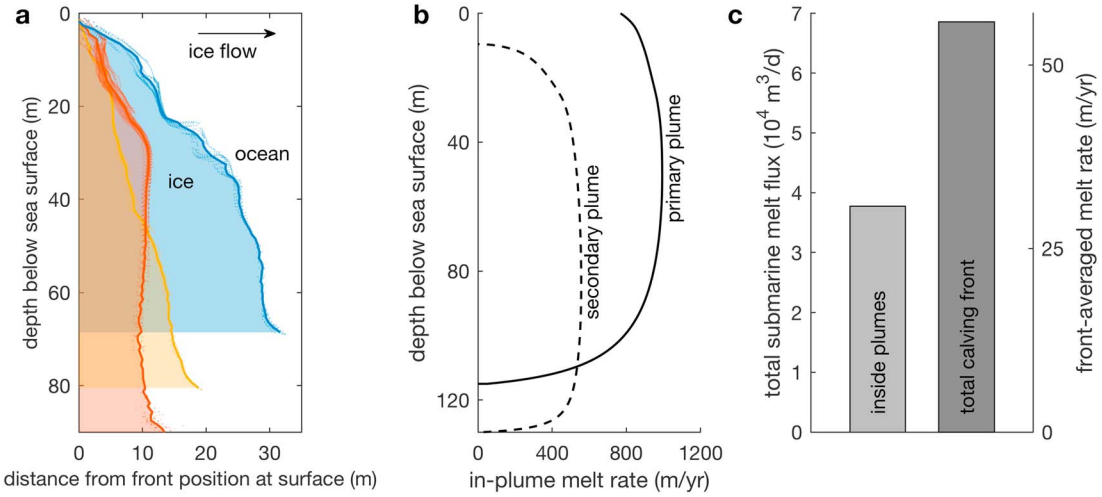


**Figure 4. Calving front shape, melting inside plumes, and total submarine melting.** (a) Calving front shape profiles (ice flow is from left to right) showing incision into the ice near the fjord surface due to high near-surface melt rates (Figures 3e–3f). The locations of the profiles are shown in Figures 1b and 3f. (b) Submarine melting inside the plumes modeled using buoyant plume theory. The secondary plume emerges from a deeper section of the calving front. (c) Total submarine meltwater flux arising from melting inside the plumes (as in (b)), and the total calving front melting.

flow are in good agreement. Below 30 m, entrainment into the vertically rising plumes drives divergent flow toward the nearest of the plumes (Figures 3a–3b).

### 3.2. Submarine Melting

Both observations (Figure 3c) and model (Figure 3d) show that water temperatures at the calving front are dominated by the ambient properties of the fjord, with a thin and warm (~6–8 °C) surface layer overlying homogeneous cooler (1 °C) water. By combining water temperature and velocity using a standard parameterization (Holland & Jenkins, 1999), we are able to estimate the submarine melt rate associated with the observed and modeled circulation (Figures 3e–3f). The swiftly-moving warm water in the near-surface induces rapid submarine melting at rates reaching 340 m/year in the model (Figure 3f). The maximum melt rate estimated from the water temperature and velocity measurements (Figure 3e) is lower at 120 m/year because the recirculating flow is found deeper in cooler waters, and we are unable to estimate melt rates in the surface 7 m where the water is warmest due to a lack of velocity measurements in this range. Below 30 m depth, elevated melt rates approaching 100 m/year are predicted where water is pulled across the calving front into the plumes.

The total melt volume estimated from the water temperature and velocity measurements (Figure 3e) is $12 \times 10^3$ m$^3$/day, which compares well with $9 \times 10^3$ m$^3$/day from the model over the same area (Figure 3f). Note once more that the measurements exclude the surface 7 m; in the model, this surface layer contributes an additional $8 \times 10^3$ m$^3$/day. We also estimate that melt-driven convection would contribute only $1 \times 10^3$ m$^3$/day over the same area (supporting information), confirming our expectation that fjord-wide circulation dominates over melt-driven convection provided the plumes are active (i.e., during the summer).

Independent evidence supporting melting due to an energetic and warm near-surface layer comes from the shape of the calving front beneath the fjord surface. Profiles from multibeam sonar in the central and western parts of the calving front, but distal from the plumes, reveal significant incision into the calving front close to the fjord surface (Figure 4a). These incisions extend to ~30 m below the surface, deeper than the warm surface water (Figures 3c–3d) but in the range of the lateral circulations (Figures 2 and 3a–3b). While we cannot completely discount the possibility these incisions are formed by calving instead of melting, we interpret the incisions to have been formed by the combination of elevated water temperature and fjord-wide circulation at the calving front, stimulating rapid melting (Figures 2 and 3). Indeed, modeled melt rates near the fjord surface exceed 300 m/year (Figure 3f) and are thus comparable to the ice velocity (Figure 1b), suggesting melting would have time to sculpt the ice without the terminus significantly advancing and potentially undergoing large calving events.

Using established buoyant plume models (Slater et al., 2016), we estimate that submarine melt rates within the primary and secondary plume reach 1,000 and 500 m/year, respectively (Figure 4b). Thus, melting within

the plumes occurs approximately an order of magnitude faster than over the rest of the calving front (Figures 3e–3f), essentially because modeled water velocities are an order of magnitude higher within the plumes. We estimate the total rate of ice loss due to melting within the plumes is $3.8 \times 10^4$ $m^3$/day (Figure 4c). However, the total mass lost due to submarine melting over the full calving front is substantially larger at $6.9 \times 10^4$ $m^3$/day (Figure 4c), indicating a significant contribution from melting driven by the fjord-wide circulation (Figures 2, 3e–3f, and 4c).

## 4. Discussion

Our observations and simulations provide the most detailed picture of near-glacier fjord circulation to date, revealing a multilayered circulation driven by the drainage of runoff from beneath the glacier. This input of runoff drives localized plumes that occupy only a small fraction of the ice-ocean contact area, yet these plumes set up fjord-wide circulations which transport warm water toward the glacier and elevate water velocities and melt rates over much of the calving front. Previous purely modeling studies (Carroll et al., 2015; Slater et al., 2015) suggest that increasing the number of plumes has a similar effect, but they focused only on melting inside of plumes. Here we have shown that plumes, although localized, nonetheless cause melting across the full calving front, comprising a substantial component of the total melt budget.

To place the estimated melt rates in the context of glacier dynamics, ice velocities exceed 300 m/year over the central 2.5 km of the calving front (Figure 1b), while the total submarine melt flux amounts to a front-average melt rate of ~55 m/year (Figure 4c). We wish to stress, however, the large uncertainties associated with the submarine melt parameterization used to estimate melt rates from water temperatures and velocities (Holland & Jenkins, 1999); this parameterization is unvalidated at tidewater glaciers and the absolute values of the estimated melt rates should therefore be viewed with caution.

While providing unprecedented spatial detail, our observations focused on circulation during a short period of the summer when subglacial runoff is high and winds are light. Numerical simulations in which the subglacial runoff is varied (supporting information) show very similar circulation to that in Figure 2, indicating that the circulation we have described is likely persistent during the summer months. It is natural to expect however that during winter, when runoff is absent, the circulation will differ substantially. Over timescales longer than covered by our observations we would also expect factors such as sea ice, icebergs, tidal mixing, and winds to influence the stratification of the fjord (Cottier et al., 2010), with feedbacks on the circulation and melt rates experienced by the glacier. A longer time series of observations would be valuable in constraining the effect of these factors on the glacier.

While some of the results presented here are specific to this system, we argue that the main finding of this study—that a localized plume will enhance melt along a much wider section of the calving front by driving a lateral circulation—is widely applicable around the ice sheet. The enhanced circulation and melting at depth (Figure 3) is an inevitable result of the entrainment of ambient water into plumes. Near the surface, the volume transport in the horizontal jet emanating from the plume increases from ~1,750 $m^3$/s adjacent to the glacier (Mankoff et al., 2016) to ~6,000 $m^3$/s at the transect CD (Figure 2c). This increase must be compensated by a return flow, in the same depth range, provided by the near-surface lateral recirculation which then generates along-glacier flow and elevates melting (Figures 2 and 3). The process is not fundamentally different if the plume, and therefore jet, equilibrate deeper in the subsurface, although the recirculation may be correspondingly deeper. Indeed, idealized simulations show that similar lateral circulations exist in fjords which are much deeper than Sarqardleq (Carroll et al., 2017). These simulations, and laboratory experiments (Whitehead, 1985), also demonstrate that the strong recirculation in Sarqarleq Fjord is not purely a result of the unique fjord shape, though further simulations would be valuable to investigate how fjord shape impacts lateral circulation-driven melting.

Like many Greenland glaciers grounded in waters shallower than 250 m (e.g., Beaird et al., 2015; Mortensen et al., 2011), Saqqarliup Sermia is not directly exposed to the warm Atlantic waters at depth which are typical of deeper-grounded glaciers (Straneo et al., 2012). Nonetheless, the deep waters inside Sarqardleq Fjord contain enough heat to drive substantial melt. The presence of warm surface waters, on the other hand, is typical of summertime conditions in Greenland (e.g., Beaird et al., 2015). In Sarqardleq Fjord, the warm surface waters combine with the near-surface lateral circulation to drive rapid melting, incising into the calving front near the fjord surface. At glaciers with warmer water at depth, it may be the deeper lateral circulation (Figure 3b, deeper than 30 m) which drives higher melting, resulting in an undercut calving front. Similarly, Greenland's

largest glaciers have ice velocities much larger than Saqqarliup Sermia. For these two reasons, the dynamic impact on calving of the fjord-scale melting may differ at other glaciers.

## 5. Conclusion

We propose that fjord-scale lateral circulation-driven melting should be considered an important ice-ocean interaction process for two reasons. First, quantification of the associated mass loss suggests that fjord-scale melting is responsible for a substantial portion of the total mass lost due to submarine melting. Compared to estimates of melting within plumes alone, this fjord-wide circulation effectively doubles the glacier-wide melt rate in Sarqardleq Fjord. Fjord-scale melting may therefore be a significant component of the calving front mass budget which ultimately determines glacier advance and retreat. Second, we suggest that the pattern of fjord-scale melting may drive a dynamic calving response of the glacier. We have attributed the near-surface notch in the calving front (Figure 4a) to rapid fjord-scale submarine melting in the upper 30 m of the fjord. Such notches are known to destabilize ice above the notch driving subaerial calving (Benn et al., 2007). The notch also creates a buoyant foot which exerts bending stresses on the ice behind, potentially promoting the opening of basal crevasses and large calving events (Benn et al., 2017; Wagner et al., 2016). Thus, the focusing of fjord-scale melting near the fjord surface may have a dynamic impact on calving and subsequent glacier retreat.

Lastly, the recognition of submarine melting as a key link between the ice sheet and ocean means there is increasing interest in coupling ice sheet and ocean models, or in finding simple ways to represent the effect of the ocean on the ice sheet. Our results suggest that fjord-scale submarine melting — driven by the fjord-scale circulation set up by localized plumes — is an important process to understand, represent, and parameterize as we move toward process-based projections of future tidewater glacier dynamics and sea level contribution.

**Acknowledgments**
Support was provided by the National Science Foundation (NSF) through PLR-1418256 and PLR-1744835, and through Woods Hole Oceanographic Institution (WHOI) Ocean and Climate Change Institute (OCCI) and the Clark Foundation. This work was also supported by a UK Natural Environmental Research Council (NERC) PhD studentship (NE/L501566/1) and Scottish Alliance for Geoscience, Environment & Society (SAGES) early career research exchange funding to D. A. S. We thank Hanumant Singh, Laura Stevens, Ken Mankoff, Rebecca Jackson, and Jeff Pietro for useful discussions and data collection.

## References

Bartholomaus, T. C., Larsen, C. F., & O'Neel, S. (2013). Does calving matter? Evidence for significant submarine melt. *Earth and Planetary Science Letters*, *380*, 21–30. https://doi.org/10.1016/j.epsl.2013.08.014

Beaird, N., Straneo, F., & Jenkins, W. (2015). Spreading of greenland meltwaters in the ocean revealed by noble gases. *Geophysical Research Letters*, *42*, 7705–7713. https://doi.org/10.1002/2015GL065003

Benn, D. I., Astrom, J., Zwinger, T., Todd, J., Nick, F. M., Cook, S., et al. (2017). Melt-under-cutting and buoyancy-driven calving from tidewater glaciers: new insights from discrete element and continuum model simulations. *Journal of Glaciology*, *63*(240), 691–702. https://doi.org/10.1017/jog.2017.41

Benn, D. I., Warren, C. R., & Mottram, R. H. (2007). Calving processes and the dynamics of calving glaciers. *Earth-Science Reviews*, *82*(3-4), 143–179. https://doi.org/10.1016/j.earscirev.2007.02.002

Box, J. E., Yang, L., Bromwich, D. H., & Bai, L. (2009). Greenland ice sheet surface air temperature variability: 1840–2007. *Journal of Climate*, *22*(14), 4029–4049. https://doi.org/10.1175/2009JCLI2816.1

Carroll, D., Sutherland, D. A., Hudson, B., Moon, T., Catania, G. A., Shroyer, E. L., et al. (2016). The impact of glacier geometry on meltwater plume structure and submarine melt in Greenland fjords. *Geophysical Research Letters*, *43*, 9739–9748. https://doi.org/10.1002/2016GL070170

Carroll, D., Sutherland, D. A., Shroyer, E. L., Nash, J. D., Catania, G. A., & Stearns, L. A. (2015). Modeling turbulent subglacial meltwater plumes: Implications for fjord-scale buoyancy-driven circulation. *Journal of Physical Oceanography*, *45*(8), 2169–2185. https://doi.org/10.1175/JPO-D-15-0033.1

Carroll, D., Sutherland, D. A., Shroyer, E. L., Nash, J. D., Catania, G. A., & Stearns, L. A. (2017). Subglacial discharge-driven renewal of tidewater glacier fjords. *Journal of Geophysical Research: Oceans*, *122*, 6611–6629. https://doi.org/10.1002/2017JC012962

Chambers, D. P., Cazenave, A., Champollion, N., Dieng, H., Llovel, W., Forsberg, R., et al. (2017). Evaluation of the global mean sea level budget between 1993 and 2014. *Surveys in Geophysics*, *38*(1), 309–327. https://doi.org/10.1007/s10712-016-9381-3

Chauché, N., Hubbard, A., Gascard, J. C., Box, J. E., Bates, R., Koppes, M., et al. (2014). Ice-ocean interaction and calving front morphology at two west Greenland tidewater outlet glaciers. *Cryosphere*, *8*, 1457–1468. https://doi.org/10.5194/tc-8-1457-2014

Cottier, F. R., Nilsen, F., Skogseth, R., Tverberg, V., Skarhamar, J., & Svendsen, H. (2010). Arctic fjords: A review of the oceanographic environment and dominant physical processes. *Geological Society, London, Special Publications*, *344*(1), 35–50. https://doi.org/10.1144/SP344.4

Cowton, T., Slater, D., Sole, A., Goldberg, D., & Nienow, P. (2015). Modeling the impact of glacial runoff on fjord circulation and submarine melt rate using a new subgrid-scale parameterization for glacial plumes. *Journal of Geophysical Research: Oceans*, *120*, 796–812. https://doi.org/10.1002/2014JC010324

Fahnestock, M., Scambos, T., Moon, T., Gardner, A., Haran, T., & Klinger, M. (2015). Rapid large-area mapping of ice flow using Landsat 8. *Remote Sensing of Environment*, *185*, 84–94. https://doi.org/10.1016/j.rse.2015.11.023

Fried, M. J., Catania, G. A., Bartholomaus, T. C., Duncan, D., Davis, M., Stearns, L. A., et al. (2015). Distributed subglacial discharge drives significant submarine melt at a Greenland tidewater glacier. *Geophysical Research Letters*, *42*, 9328–9336. https://doi.org/10.1002/2015GL065806

Fried, M. J., Catania, G. A., Stearns, L. A., Sutherland, D. A., Bartholomaus, T. C., Shroyer, E., & Nash, J. (2018). Reconciling drivers of seasonal terminus advance and retreat at 13 Central West Greenland tidewater glaciers. *Journal of Geophysical Research: Earth Surface*, *123*, 1590–1607. https://doi.org/10.1029/2018JF004628

Holland, D. M., & Jenkins, A. (1999). Modeling thermodynamic ice-ocean interactions at the base of an ice shelf. *Journal of Physical Oceanography*, *29*(8), 1787–1800. https://doi.org/10.1175/1520-0485(1999)029<1787:MTIOIA>2.0.CO;2

Holland, D. M., Thomas, R. H., de Young, B., Ribergaard, M. H., & Lyberth, B. (2008). Acceleration of Jakobshavn Isbrae triggered by warm subsurface ocean waters. *Nature Geoscience*, *1*(10), 659–664. https://doi.org/10.1038/ngeo316

Jackson, R. H., Shroyer, E. L., Nash, J. D., Sutherland, D. A., Carroll, D., Fried, M. J., et al. (2017). Near-glacier surveying of a subglacial discharge plume: Implications for plume parameterizations. *Geophysical Research Letters*, *44*, 6886–6894. https://doi.org/10.1002/2017GL073602

Jenkins, A. (2011). Convection-driven melting near the grounding lines of ice shelves and tidewater glaciers. *Journal of Physical Oceanography*, *41*(12), 2279–2294. https://doi.org/10.1175/JPO-D-11-03.1

Kimball, P. W., Bailey, J., Das, S. B., Geyer, R., Harrison, T., Kunz, C., et al. (2014). The WHOI Jetyak: An autonomous surface vehicle for oceanographic research in shallow or dangerous waters. In *IEEE/OES Autonomous Underwater Vehicles (AUV)*, United States, pp. 1–7. https://doi.org/10.1109/AUV.2014.7054430

Large, W. G., McWilliams, J. C., & Doney, S. C. (1994). Oceanic vertical mixing: A review and a model with a nonlocal boundary layer parameterization. *Reviews of Geophysics*, *32*(4), 363–403. https://doi.org/10.1029/94RG01872

Luckman, A., Benn, D. I., Cottier, F., Bevan, S., Nilsen, F., & Inall, M. (2015). Calving rates at tidewater glaciers vary strongly with ocean temperature. *Nature Communications*, *6*, 8566. https://doi.org/10.1038/ncomms9566

Magorrian, S. J., & Wells, A. J. (2016). Turbulent plumes from a glacier terminus melting in a stratified ocean. *Journal of Geophysical Research: Oceans*, *121*, 4670–4696. https://doi.org/10.1002/2015JC011160

Mankoff, K. D., Straneo, F., Cenedese, C., Das, S. B., Richards, C. G., & Singh, H. (2016). Structure and dynamics of a subglacial discharge plume in a Greenlandic fjord. *Journal of Geophysical Research: Oceans*, *121*, 8670–8688. https://doi.org/10.1002/2016JC011764

Marshall, J., Hill, C., Perelman, L., & Adcroft, A. (1997). Hydrostatic, quasi-hydrostatic, and nonhydrostatic ocean modeling. *Journal of Geophysical Research*, *102*(C3), 5733–5752. https://doi.org/10.1029/96JC02776

Moon, T., Joughin, I., Smith, B., & Howat, I. (2012). 21st-century evolution of Greenland outlet glacier velocities. *Science*, *336*(6081), 576–578. https://doi.org/10.1126/science.1219985

Moon, T., Sutherland, D., Carroll, D., Felikson, D., Kehrl, L., & Straneo, F. (2018). Subsurface iceberg melt key to Greenland fjord freshwater budget. *Nature Geoscience*, *11*(1), 49–54. https://doi.org/10.1038/s41561-017-0018-z

Morlighem, M., Bondzio, J., Seroussi, H., Rignot, E., Larour, E., Humbert, A., & Rebuffi, S. (2016). Modeling of Store Gletscher's calving dynamics, West Greenland, in response to ocean thermal forcing. *Geophysical Research Letters*, *43*, 2659–2666. https://doi.org/10.1002/2016GL067695

Mortensen, J., Lennert, K., Bendtsen, J., & Rysgaard, S. (2011). Heat sources for glacial melt in a sub-Arctic fjord (Godthabsfjord) in contact with the Greenland ice sheet. *Journal of Geophysical Research*, *116*, C01013. https://doi.org/10.1029/2010JC006528

Motyka, R. J., Hunter, L., Echelmeyer, K. A., & Connor, C. (2003). Submarine melting at the terminus of a temperate tidewater glacier, LecConte Glacier, Alaska, USA. *Annals of Glaciology*, *36*(1), 57–65. https://doi.org/10.3189/172756403781816374

Nick, F. M., Vieli, A., Andersen, M. L., Joughin, I., Payne, A., Edwards, T. L., et al. (2013). Future sea-level rise from Greenland's main outlet glaciers in a warming climate. *Nature*, *497*, 235–238. https://doi.org/10.1038/nature12068

O'Leary, M., & Christoffersen, P. (2013). Calving on tidewater glaciers amplified by submarine frontal melting. *The Cryosphere*, *7*(1), 119–128. https://doi.org/10.5194/tc-7-119-2013

Rignot, E., Fenty, I., Xu, Y., Cai, C., & Kemp, C. (2015). Undercutting of marine-terminating glaciers in West Greenland. *Geophysical Research Letters*, *42*, 5909–5917. https://doi.org/10.1002/2015GL064236

Rignot, E., Xu, Y., Menemenlis, D., Mouginot, J., Scheuchl, B., Li, X., et al. (2016). Modeling of ocean-induced ice melt rates of five West Greenland glaciers over the past two decades. *Geophysical Research Letters*, *43*, 6374–6382. https://doi.org/10.1002/2016GL068784

Scambos, T., Fahnestock, M., Moon, T., Gardner, A., & Klinger, M. (2016). *Global land ice velocity extraction from Landsat 8 (GoLIVE), Version 1*. Boulder, Colorado USA: NSIDC: National Snow and Ice Data Center. https://doi.org/10.7265/N5ZP442B

Slater, D. A., Goldberg, D. N., Nienow, P. W., & Cowton, T. R. (2016). Scalings for submarine melting at tidewater glaciers from buoyant plume theory. *Journal of Physical Oceanography*, *46*(6), 1839–1855. https://doi.org/10.1175/JPO-D-15-0132.1

Slater, D. A., Nienow, P. W., Cowton, T. R., Goldberg, D. N., & Sole, A. J. (2015). Effect of near-terminus subglacial hydrology on tidewater glacier submarine melt rates. *Geophysical Research Letters*, *42*, 2861–2868. https://doi.org/10.1002/2014GL062494

Slater, D. A., Nienow, P. W., Goldberg, D. N., Cowton, T. R., & Sole, A. J. (2017). A model for tidewater glacier undercutting by submarine melting. *Geophysical Research Letters*, *44*, 2360–2368. https://doi.org/10.1002/2016GL072374

Smagorinsky, J. (1963). General ciculation experiments with the primitive equations. *Monthly Weather Review*, *91*(3), 99. https://doi.org/10.1175/1520-0493(1963)091<0099:GCEWTP>2.3.CO;2

Stevens, L. A., Straneo, F., Das, S. B., Plueddemann, A. J., Kukulya, A. L., & Morlighem, M. (2016). Linking glacially modified waters to catchment-scale subglacial discharge using autonomous underwater vehicle observations. *The Cryosphere*, *10*(1), 417–432. https://doi.org/10.5194/tc-10-417-2016

Straneo, F., Curry, R. G., Sutherland, D. A., Hamilton, G. S., Cenedese, C., Vage, K., & Stearns, L. A. (2011). Impact of fjord dynamics and glacial runoff on the circulation near Helheim Glacier. *Nature Geoscience*, *4*(5), 322–327. https://doi.org/10.1038/ngeo1109

Straneo, F., & Heimbach, P. (2013). North Atlantic warming and the retreat of Greenland's outlet glaciers. *Nature*, *504*, 36–43. https://doi.org/10.1038/nature12854

Straneo, F., Sutherland, D. A., Holland, D., Gladish, C., Hamilton, G. S., Johnson, H. L., et al. (2012). Characteristics of ocean waters reaching Greenland's glaciers. *Annals of Glaciology*, *53*(60), 202–210. https://doi.org/10.3189/2012AoG60A059

Todd, J., Christoffersen, P., Zwinger, T., Raback, P., Chauche, N., Benn, D., et al. (2018). A full-stokes 3D calving model applied to a large Greenlandic glacier. *Journal of Geophysical Research: Earth Surface*, *123*, 410–432. https://doi.org/10.1002/2017JF004349

van den Broeke, M. R., Enderlin, E. M., Howat, I. M., Kuipers Munneke, P., Noel, B. P. Y., van de Berg, W. J., & Wouters, B. (2016). On the recent contribution of the Greenland ice sheet to sea level change. *The Cryosphere*, *10*(5), 1933–1946. https://doi.org/10.5194/tc-10-1933-2016

Wagner, T. J. W., James, T. D., Murray, T., & Vella, D. (2016). On the role of buoyant flexure in glacier calving. *Geophysical Research Letters*, *43*, 232–240. https://doi.org/10.1002/2015GL067247

Whitehead, J. A. (1985). The deflection of a baroclinic jet by a wall in a rotating fluid. *Journal of Fluid Mechanics*, *157*, 79–93. https://doi.org/10.1017/S0022112085002312

Xie, S., Dixon, T. H., Voytenko, D., Holland, D. M., Holland, D., & Zheng, T. (2016). Precursor motion to iceberg calving at Jakobshavn Isbrae, Greenland, observed with terrestrial radar interferometry. *Journal of Glaciology*, *62*(236), 1134–1142. https://doi.org/10.1017/jog.2016.104

Xu, Y., Rignot, E., Menemenlis, D., & Koppes, M. (2012). Numerical experiments on subaqueous melting of Greenland tidewater glaciers in response to ocean warming and enhanced subglacial discharge. *Annals of Glaciology*, *53*(60), 229–234. https://doi.org/10.3189/2012AoG60A139

Yin, J., Overpeck, J. T., Griffies, S. M., Hu, A., Russell, J. L., & Stouffer, R. J. (2011). Different magnitudes of projected subsurface ocean warming around Greenland and Antarctica. *Nature Geoscience*, *4*(8), 524–528. https://doi.org/10.1038/ngeo1189